Universität Karlsruhe (TH)
Institut für Baustatik

A piezoelectric solid shell element based on a mixed variational formulation for geometrically linear and nonlinear applications

S. Klinkel, W. Wagner

Mitteilung 3(2006)

Universität Karlsruhe (TH)
Institut für Baustatik

A piezoelectric solid shell element based on a mixed variational formulation for geometrically linear and nonlinear applications

S. Klinkel, W. Wagner

Mitteilung 3(2006)

Prof. Dr.–Ing. W. Wagner
Institut für Baustatik
Universität Karlsruhe
Postfach 6980
76128 Karlsruhe

Telefon: (0721) 608–2280
Telefax: (0721) 608–6015
E–mail: bs@.uni-karlsruhe.de
Internet: http://www.bs.uni-karlsruhe.de

A piezoelectric solid shell element based on a mixed variational formulation for geometrically linear and nonlinear applications

Sven Klinkel, Werner Wagner

Institut für Baustatik, Universität Karlsruhe (TH), Kaiserstr. 12, 76131 Karlsruhe, Germany

Abstract The paper is focused on a piezoelectric solid shell finite element formulation. A geometrically non-linear theory allows large deformations and includes stability problems. The formulation is based on a variational principle of the Hu-Washizu type including six independent fields: displacements, electric potential, strains, electric field, mechanical stresses and dielectric displacements. The element has 8 nodes with displacements and the electric potential as nodal degrees of freedom. A bilinear distribution through the thickness of the electric field is assumed to obtain correct results in bending dominated situations. The presented element is able to model arbitrary curved shells and incorporates a 3D-material law. Numerical examples demonstrate the ability of the proposed model to analyze piezoelectric devices.

1 Introduction

In recent years several new shell elements have been proposed, where piezoelectric constitutive relations have been included in the underlying element formulation. One may distinguish between element formulations, which model a reference surface of the shell structure, see e.g. [1, 2, 3, 4, 5, 6], and solid shell elements which model the top and bottom surfaces of structures, see e. g. [7, 8, 9, 10, 11, 12]. Some of these element formulations are restricted to shallow shell structures, [5, 6], where the initial shell curvature is assumed to be small. Due to the fact that the piezoelectric devices have traditionally laminate forms, the above mentioned shell formulations include a more or less sophisticated laminate theory. The solid shell elements circumvent complicated laminate theories by modeling each ply in a laminate with one element in thickness direction.

In Refs. [8, 13, 14] it is pointed out that geometrically nonlinear characteristics can significantly influence the performance of piezoelectric structures and systems. Geometrically nonlinear effects like buckling of plates and snap-through behavior were analyzed in [1, 6, 15, 16]. A lot of nonlinear piezoelectric plate formulations [6, 13, 14, 15, 16] are based on von Kármán plate theory, which is a nonlinear theory of lowest order. A geometrically nonlinear theory which incorporates large rotations is presented in [1, 7, 8].

A common assumption in piezoelectric models is that the electric field is constant through the thickness inside the actuator or sensor. This is in bending dominated situations not correct. Benjeddou et al. [17] emphasized that a quadratic electric potential through the plate thickness satisfies the electric charge conservation law exactly. A quadratic approximation leads to additional degrees of freedom, see e. g. [2, 3, 4, 18]. This is also the case in [5], where a hybrid finite shell formulation with degrees of freedom for the electric potential and the dielectric displacements is suggested.

Hybrid and mixed approaches are found in [10, 11, 19, 20]. The most general variational principle which includes six field variables is considered in [20]. From this general princi-

ple here some degenerated principles are derived, which are employed for the finite element formulation.

The main features and novel aspects of the present formulation are summarized as follows:

- The finite element formulation is based on the most general variational formulation principle of the Hu-Wahizu type and includes six independently assumed field variables: the stress field, the strain field, the displacements, the electric displacements, the electric field, and the electric potential. Each field is incorporated in the finite element formulation and is approximated with appropriate interpolations on element level. In contrast to [7, 21] an orthogonality between the stress and strain approximations is assumed.
- A bilinear approximation of the electric field through the shell thickness is assumed, which is necessary to pass the out of plane bending patch test.
- A complete geometrically nonlinear theory is presented. It allows large deformations and accounts for snap-through effects and stability problems. In contrast to shallow shells [1, 5, 6] the presented finite shell element is able to model arbitrary curved shell structures.

The paper is organized as follows: In Section 2 we introduce the gradient fields in a curvilinear description. For the strain measure a geometrically nonlinear kinematic assumption is employed. In Section 3 the constitutive relations are presented following by Section 4, where the variational principle is introduced. Then Section 5 is concerned with the mixed finite element approximation. In the last Section some numerical examples demonstrate the ability of the proposed model.

2 Gradient fields

In this section the Green-Lagrangean strains and the electric field are derived in convective co-ordinates. The parameter ξ^3 is defined as thickness co-ordinate and ξ^1, ξ^2 as in-plane co-ordinates of the considered shell formulation. The position vector of the reference configuration $\mathcal{B}_0$ and the current configuration $\mathcal{B}_t$ are denoted by $\boldsymbol{X}$ and $\boldsymbol{x} = \boldsymbol{X} + \boldsymbol{u}$, where $\boldsymbol{u}$ is the displacement vector. The co-variant tangent vectors are defined as $\boldsymbol{G}_i = \frac{\partial \boldsymbol{X}}{\partial \xi^i}$, $\boldsymbol{g}_i = \frac{\partial \boldsymbol{x}}{\partial \xi^i}$ with $i = 1, 2, 3$. Introducing the metric coefficients $g_{ij} = \boldsymbol{g}_i \cdot \boldsymbol{g}_j$ and $G_{ij} = \boldsymbol{G}_i \cdot \boldsymbol{G}_j$ the Green-Lagrangean strain components read

$$E_{ij} = \frac{1}{2}(g_{ij} - G_{ij}) \quad , \tag{1}$$

and are arranged in a vector $\boldsymbol{E}_c = [E_{11},\, E_{22},\, E_{33},\, 2E_{12},\, 2E_{13},\, 2E_{23}]^T$. Introducing

$$\boldsymbol{T} = \begin{bmatrix} (J_{11})^2 & (J_{12})^2 & (J_{13})^2 & aJ_{11}J_{12} & aJ_{11}J_{13} & aJ_{12}J_{13} \\ (J_{21})^2 & (J_{22})^2 & (J_{23})^2 & aJ_{21}J_{22} & aJ_{21}J_{23} & aJ_{22}J_{23} \\ (J_{31})^2 & (J_{32})^2 & (J_{33})^2 & aJ_{31}J_{32} & aJ_{31}J_{33} & aJ_{32}J_{33} \\ bJ_{11}J_{21} & bJ_{12}J_{22} & bJ_{13}J_{23} & J_{11}J_{22} + J_{12}J_{21} & J_{11}J_{23} + J_{13}J_{21} & J_{12}J_{23} + J_{13}J_{22} \\ bJ_{11}J_{31} & bJ_{12}J_{32} & bJ_{13}J_{33} & J_{11}J_{32} + J_{12}J_{31} & J_{11}J_{33} + J_{13}J_{31} & J_{12}J_{33} + J_{13}J_{32} \\ bJ_{21}J_{31} & bJ_{22}J_{32} & bJ_{23}J_{33} & J_{21}J_{32} + J_{22}J_{31} & J_{21}J_{33} + J_{23}J_{31} & J_{22}J_{33} + J_{23}J_{32} \end{bmatrix}, \tag{2}$$

the transformation matrix is defined as $\boldsymbol{T}_S = \boldsymbol{T}$ with $a = 1$, $b = 2$, $J_{ik} = \boldsymbol{G}_i \cdot \boldsymbol{t}_k$ and $\boldsymbol{t}_1 = \frac{\boldsymbol{G}_1}{\|\boldsymbol{G}_1\|}$, $\boldsymbol{t}_2 = \frac{\boldsymbol{G}_3 \times \boldsymbol{G}_1}{\|\boldsymbol{G}_3 \times \boldsymbol{G}_1\|}$, $\boldsymbol{t}_3 = \boldsymbol{t}_1 \times \boldsymbol{t}_2$, the transformation to the local orthonormal basis system $\boldsymbol{t}_i$ is given as $\boldsymbol{E} = \boldsymbol{T}_S^{-1}\, \boldsymbol{E}_c$. The covariant components of the electric field are also arranged in a vector $\vec{\boldsymbol{E}}_c = [\vec{E}_1,\, \vec{E}_2,\, \vec{E}_3]^T$ with

$$\vec{E}_i = -\frac{\partial \varphi}{\partial \xi^i}, \tag{3}$$

here φ denotes the electric potential. With the Jacobian matrix $\boldsymbol{J}$ the transformation to the local orthonormal basis system is determined by $\vec{\boldsymbol{E}} = \boldsymbol{J}^{-1} \vec{\boldsymbol{E}}_c$. The strains and the electric field are arranged in the vector $\boldsymbol{\varepsilon}^T = \left[\boldsymbol{E}^T \vec{\boldsymbol{E}}^T\right]$.

3 Constitutive equations

The relation between stresses, dielectric displacements, strains, and the electric field is assumed to be

$$\boldsymbol{\sigma} = \mathbb{D}\, \boldsymbol{\varepsilon} \quad \text{with} \quad \mathbb{D} = \begin{bmatrix} \mathbb{C} & -\mathbb{e} \\ -\mathbb{e}^T & -\boldsymbol{\epsilon} \end{bmatrix} \quad . \tag{4}$$

In Eq. (4) the vector $\boldsymbol{\sigma}$ is defined as $\boldsymbol{\sigma}^T = [\boldsymbol{S}^T,\, -\vec{\boldsymbol{D}}^T]$, where $\boldsymbol{S}$ is the stress vector and $\vec{\boldsymbol{D}}$ the vector of dielectric displacements. The constant material matrix $\mathbb{D}$ contains the elasticity matrix $\mathbb{C}$, the piezoelectric matrix $\mathbb{e}$ and the permittivity matrix $\boldsymbol{\epsilon}$. A detailed description of the material constants is given in the Appendix. The stored energy function is defined as $W_0 = \frac{1}{2}\, \boldsymbol{\varepsilon}^T \mathbb{D} \boldsymbol{\varepsilon}$.

4 Variational formulation

In this section a variational functional of the Hu-Washizu type with six independent fields is introduced as

$$\begin{aligned} \Pi(\boldsymbol{u},\, \varphi,\, \bar{\boldsymbol{\varepsilon}},\, \widetilde{\boldsymbol{\sigma}}) = & \int_{\mathcal{B}_0} W_0(\bar{\boldsymbol{\varepsilon}}) - \widetilde{\boldsymbol{\sigma}} \cdot (\bar{\boldsymbol{\varepsilon}} - \boldsymbol{\varepsilon})\, \mathrm{dV} \\ & - \int_{\mathcal{B}_0} \boldsymbol{b} \cdot \boldsymbol{u}\, \mathrm{dV} - \int_{\partial_t \mathcal{B}_0} \boldsymbol{t} \cdot \boldsymbol{u}\, \mathrm{dA} + \int_{\partial_q \mathcal{B}_0} \mathrm{q}\, \varphi\, \mathrm{dA}\,, \end{aligned} \tag{5}$$

where $\widetilde{\boldsymbol{\sigma}}$, $\bar{\boldsymbol{\varepsilon}}$ are functions of the independent quantities $\widetilde{\boldsymbol{S}}$, $\widetilde{\vec{\boldsymbol{D}}}$, $\bar{\boldsymbol{E}}$, and $\bar{\vec{\boldsymbol{E}}}$. The body forces $\boldsymbol{b}$ are defined in the reference configuration $\mathcal{B}_0$ and $\boldsymbol{t}$ is the prescribed traction vector on the boundary $\partial_t \mathcal{B}_0$. The electric surface charge q is prescribed on the boundary $\partial_q \mathcal{B}_0$. Let $\mathcal{U} := \{\delta \boldsymbol{u} \in [H^1(\mathcal{B}_0)]^3 \delta \boldsymbol{u}|_{\partial_u \mathcal{B}_0} = 0\}$ be the space of admissible displacement variations and $\mathcal{V} := \{\delta\varphi \in [H^1(\mathcal{B}_0)]^3\ \delta\varphi|_{\partial_\varphi \mathcal{B}_0} = 0\}$ be the space of admissible electric potential variations. Further let $\widetilde{\mathcal{S}} = \bar{\mathcal{E}} = [L_2(\mathcal{B}_0)]$ the spaces of admissible variations of the variables $\bar{\boldsymbol{\varepsilon}}$, $\widetilde{\boldsymbol{\sigma}}$. The

first variation reads

$$\begin{aligned}\delta\Pi = & \int_{\mathcal{B}_0} \delta\bar{\boldsymbol{\varepsilon}} \cdot \big(\frac{\partial W_0}{\partial \bar{\boldsymbol{\varepsilon}}} - \widetilde{\boldsymbol{\sigma}}\big)\, \mathrm{dV} + \int_{\mathcal{B}_0} \delta\widetilde{\boldsymbol{\sigma}} \cdot \big(\boldsymbol{\varepsilon} - \bar{\boldsymbol{\varepsilon}}\big)\, \mathrm{dV} \\ & + \int_{\mathcal{B}_0} \delta\boldsymbol{\varepsilon} \cdot \widetilde{\boldsymbol{\sigma}} - \delta\boldsymbol{u} \cdot \boldsymbol{b}\, \mathrm{dV} - \int_{\partial_\mathrm{t}\mathcal{B}_0} \delta\boldsymbol{u} \cdot \boldsymbol{t}\, \mathrm{dA} + \int_{\partial_\mathrm{q}\mathcal{B}_0} \delta\varphi\, \mathrm{q}\, \mathrm{dA} \;= 0 \quad .\end{aligned} \tag{6}$$

The variation of the strains and the electric field result in

$$\delta E_{ij} = \frac{1}{2}\big(\frac{\delta\boldsymbol{u}}{\xi^i} \cdot \boldsymbol{g}_j + \boldsymbol{g}_i \cdot \frac{\delta\boldsymbol{u}}{\xi^j}\big) \quad , \quad \delta\vec{E}_i = \frac{\delta\varphi}{\xi^i} \quad . \tag{7}$$

The weak form is solved iteratively by employing Newton-Raphson's method. This requires the linearization of Eq. (6), which reads

$$\begin{aligned}\mathrm{D}[\delta\Pi] \cdot (\Delta\boldsymbol{u},\, \Delta\varphi,\, \Delta\bar{\boldsymbol{\varepsilon}},\, \Delta\widetilde{\boldsymbol{\sigma}}) = & \int_{\mathcal{B}_0} \delta\bar{\boldsymbol{\varepsilon}} \cdot \frac{\partial\partial W_0}{\partial\bar{\boldsymbol{\varepsilon}}\,\partial\bar{\boldsymbol{\varepsilon}}}\Delta\bar{\boldsymbol{\varepsilon}} \;-\; \delta\bar{\boldsymbol{\varepsilon}} \cdot \Delta\widetilde{\boldsymbol{\sigma}}\, \mathrm{dV} \\ & + \int_{\mathcal{B}_0} \delta\widetilde{\boldsymbol{\sigma}} \cdot \Delta\boldsymbol{\varepsilon} \;-\; \delta\widetilde{\boldsymbol{\sigma}} \cdot \Delta\bar{\boldsymbol{\varepsilon}}\, \mathrm{dV} + \int_{\mathcal{B}_0} \delta\boldsymbol{\varepsilon} \cdot \Delta\widetilde{\boldsymbol{\sigma}} \;+\; \widetilde{\boldsymbol{\sigma}} \cdot \Delta\delta\boldsymbol{\varepsilon}\, \mathrm{dV} \quad ,\end{aligned} \tag{8}$$

with $\Delta\delta\boldsymbol{\varepsilon} = [\Delta\delta\boldsymbol{E}^T,\, \boldsymbol{0}]^T$ and $\Delta\delta E_{ij} = \frac{1}{2}(\frac{\delta\boldsymbol{u}}{\xi^i} \cdot \frac{\Delta\boldsymbol{u}}{\xi^j} + \frac{\Delta\boldsymbol{u}}{\xi^i} \cdot \frac{\delta\boldsymbol{u}}{\xi^j})$.

5 Finite element approximations

The finite element approximation is constructed in the sense that the whole domain is divided in element domains with $\mathcal{B} = \cup_{e=1}^{nelm}\mathcal{B}_e$, where $nelm$ is the total number of elements. The geometry, displacements and electric potential are approximated as $\boldsymbol{X}_e^h = \sum_{I=1}^{8} N_I\, \boldsymbol{X}_I$, $\boldsymbol{u}_e^h = \sum_{I=1}^{8} N_I\, \boldsymbol{u}_I$ and $\varphi_e^h = \sum_{I=1}^{8} N_I\, \varphi_I$ with the same interpolation functions $N_I = \frac{1}{8}(1 + \xi_I^1\xi^1)(1 + \xi_I^2\xi^2)(1 + \xi_I^3\xi^3)$, $-1 \le \xi^i \le +1$ at nodes $I = 1, 2, 3, ..., 8$. The vectors $\boldsymbol{X}_I$, $\boldsymbol{u}_I$ contain the nodal co-ordinates and displacements, respectively. Arranging N_I in the matrix $\boldsymbol{N} = [\boldsymbol{N}_1,\, \boldsymbol{N}_2,\, \boldsymbol{N}_3,\, \boldsymbol{N}_4,\, \boldsymbol{N}_5,\, \boldsymbol{N}_6,\, \boldsymbol{N}_7,\, \boldsymbol{N}_8]$ with $\boldsymbol{N}_I = \mathrm{diag}[N_I,\, N_I,\, N_I,\, N_I]$, the virtual quantities are interpolated as

$$\begin{bmatrix} \delta\boldsymbol{u}_e^h \\ \delta\phi_e^h \end{bmatrix} = \boldsymbol{N}\, \delta\boldsymbol{v}_e \quad , \tag{9}$$

where $\boldsymbol{v}_e^T = [\boldsymbol{v}_1^T,\, \boldsymbol{v}_2^T,\, \boldsymbol{v}_3^T,\, ...,\, \boldsymbol{v}_8^T]$ is the vector of nodal degrees of freedom with $\boldsymbol{v}_I^T = [u_1,\, u_2,\, u_3,\, \varphi]_I^T$. Accordingly, δbv_e is the vector of the virtual values. The approximation of the virtual gradient field $\boldsymbol{\varepsilon}$ reads

$$\delta\boldsymbol{\varepsilon}_e^h = \boldsymbol{B}\, \delta\boldsymbol{v}_e \tag{10}$$

with $\boldsymbol{B} = [\boldsymbol{B}_1,\, \boldsymbol{B}_2,\, \boldsymbol{B}_3,\, \boldsymbol{B}_4,\, \boldsymbol{B}_5,\, \boldsymbol{B}_6,\, \boldsymbol{B}_7,\, \boldsymbol{B}_8]$ and $\boldsymbol{B}_I = \begin{bmatrix} \boldsymbol{B}_I^u & \boldsymbol{0} \\ \boldsymbol{0} & \boldsymbol{B}_I^\phi \end{bmatrix}$.

The matrix $\boldsymbol{B}_I^u$ is defined with some assumed natural strain (ANS) interpolations, see [22, 23], as

$$\boldsymbol{B}_I^u = \boldsymbol{T}_S^{-1} \begin{bmatrix} N_{I,1}\,\boldsymbol{g}_1^{hT} \\ N_{I,2}\,\boldsymbol{g}_2^{hT} \\ \sum_{L=i}^{iv} \frac{1}{4}(1+\xi^{1\,L}\,\xi^1)(1+\xi^{2\,L}\,\xi^2)\,N_{I,3}\,(\boldsymbol{g}_3^L)^T \\ N_{I,1}\,\boldsymbol{g}_2^{hT} + N_{I,2}\,\boldsymbol{g}_1^{hT} \\ \frac{1}{2}(1-\xi^2)(N_{I,1}^B\,(\boldsymbol{g}_3^B)^T + N_{I,3}^B\,(\boldsymbol{g}_1^B)^T) + \frac{1}{2}(1+\xi^2)(N_{I,1}^D\,(\boldsymbol{g}_3^D)^T + N_{I,3}^D\,(\boldsymbol{g}_1^D)^T) \\ \frac{1}{2}(1-\xi^1)(N_{I,2}^A\,(\boldsymbol{g}_3^A)^T + N_{I,3}^A\,(\boldsymbol{g}_2^A)^T) + \frac{1}{2}(1+\xi^1)(N_{I,2}^C\,(\boldsymbol{g}_3^C)^T + N_{I,3}^C\,(\boldsymbol{g}_2^C)^T) \end{bmatrix}, \tag{11}$$

The matrix $\boldsymbol{B}_I^\phi$ at the node I is determined by

$$\boldsymbol{B}_I^\phi = \boldsymbol{J}^{-1} \begin{bmatrix} N_{I,\xi^1} & N_{I,\xi^2} & N_{I,\xi^3} \end{bmatrix}^T \quad . \tag{12}$$

In the linearized weak form Eq. (8) the quantity $\widetilde{\boldsymbol{\sigma}} \cdot \Delta\delta\boldsymbol{\varepsilon}$ appears, which is approximated as $(\widetilde{\boldsymbol{\sigma}} \cdot \Delta\delta\boldsymbol{\varepsilon})^h = \delta\boldsymbol{v}_e^T\,\boldsymbol{G}\,\Delta\boldsymbol{v}_e$. The matrix $\boldsymbol{G}$ is partitioned as

$$\boldsymbol{G} = \begin{bmatrix} \boldsymbol{G}_{11} & \boldsymbol{G}_{12} & \cdots & \boldsymbol{G}_{18} \\ \boldsymbol{G}_{21} & \boldsymbol{G}_{22} & \cdots & \boldsymbol{G}_{28} \\ \vdots & \vdots & \ddots & \vdots \\ \boldsymbol{G}_{81} & \boldsymbol{G}_{82} & \cdots & \boldsymbol{G}_{88} \end{bmatrix} \tag{13}$$

with $\boldsymbol{G}_{IJ} = \mathrm{diag}[G_{IJ},\, G_{IJ},\, G_{IJ},\, 0]$. Considering the ANS interpolations and the transformation (2) the scalar G_{IJ} is obtained as

$$G_{IJ} = (\widetilde{\boldsymbol{S}}_e^h)^T\,\boldsymbol{T}_S^{-1} \begin{bmatrix} N_{I,1}N_{J,1} \\ N_{I,2}N_{J,2} \\ \sum_{L=i}^{iv} \frac{1}{4}(1+\xi^{1\,L}\,\xi^1)(1+\xi^{2\,L}\,\xi^2)\,N_{I,3}N_{J,3} \\ N_{I,1}N_{J,2} + N_{I,2}N_{J,1} \\ \frac{1}{2}[(1-\xi^2)\,(N_{I,1}^B N_{J,3}^B + N_{I,3}^B N_{J,1}^B) + (1+\xi^2)\,(N_{I,1}^D N_{J,3}^D + N_{I,3}^D N_{J,1}^D)] \\ \frac{1}{2}[(1-\xi^1)\,(N_{I,2}^A N_{J,3}^A + N_{I,3}^A N_{J,2}^A) + (1+\xi^1)\,(N_{I,2}^C N_{J,3}^C + N_{I,3}^C N_{J,2}^C)] \end{bmatrix}. \tag{14}$$

Here, $\widetilde{\boldsymbol{S}}_e^h$ denotes the approximation of the stress field $\widetilde{\boldsymbol{S}}$ on element level, see below.

The independent field $\bar{\boldsymbol{\varepsilon}}$ is additively split in two parts, which are approximated with the following interpolations

$$\bar{\boldsymbol{\varepsilon}}_e^h = \boldsymbol{M}_\alpha^1\,\boldsymbol{\alpha}^1 + \boldsymbol{M}_\alpha^2\,\boldsymbol{\alpha}^2 \text{ with } \boldsymbol{M}_\alpha^1 = \begin{bmatrix} \boldsymbol{N}_E & \boldsymbol{0} \\ \boldsymbol{0} & \boldsymbol{N}_{\vec{E}} \end{bmatrix},\ \boldsymbol{M}_\alpha^2 = \begin{bmatrix} \boldsymbol{M}_E & \boldsymbol{0} \\ \boldsymbol{0} & \boldsymbol{M}_{\vec{E}} \end{bmatrix}, \tag{15}$$

where $\boldsymbol{\alpha}^1 \in \mathbb{R}^{30}$ and $\boldsymbol{\alpha}^2 \in \mathbb{R}^{10}$. The matrices $\boldsymbol{N}_E$, $\boldsymbol{N}_{\vec{E}}$ are given as

$$\boldsymbol{N}_E = (\boldsymbol{T}_E^0)^T \left[\mathbf{1},\ \begin{array}{cccccccccccc} & \xi^3 & \xi^2\xi^3 & 0 & 0 & 0 & \xi^2 & 0 & 0 & 0 & 0 & 0 & 0 \\ & 0 & 0 & \xi^3 & \xi^1\xi^3 & 0 & 0 & \xi^1 & 0 & 0 & 0 & 0 & 0 \\ & 0 & 0 & 0 & 0 & 0 & 0 & 0 & \xi^1 & \xi^2 & \xi^1\xi^2 & 0 & 0 \\ & 0 & 0 & 0 & 0 & \xi^3 & 0 & 0 & 0 & 0 & 0 & 0 & 0 \\ & 0 & 0 & 0 & 0 & 0 & 0 & 0 & 0 & 0 & 0 & \xi^2 & 0 \\ & 0 & 0 & 0 & 0 & 0 & 0 & 0 & 0 & 0 & 0 & 0 & \xi^1 \end{array}\right] \tag{16}$$

$$\boldsymbol{N}_{\vec{E}} = \boldsymbol{J}_0^T \begin{bmatrix} 1 & 0 & 0 & \xi^2 & \xi^3 & \xi^2\xi^3 & 0 & 0 & 0 & 0 & 0 & 0 \\ 0 & 1 & 0 & 0 & 0 & 0 & \xi^1 & \xi^3 & \xi^1\xi^3 & 0 & 0 & 0 \\ 0 & 0 & 1 & 0 & 0 & 0 & 0 & 0 & 0 & \xi^1 & \xi^2 & \xi^1\xi^2 \end{bmatrix} \quad . \tag{17}$$

Quantities, which are evaluated at the element center are denoted with the index 0 and $\mathbf{1}$ is a 6×6 identity matrix. The transformation matrix $\boldsymbol{T}_E$ is obtained by Eq. (2) considering $a = 2$ and $b = 1$. The matrices $\boldsymbol{M}_E$, $\boldsymbol{M}_{\vec{E}}$ are defined as

$$\boldsymbol{M}_E = \frac{\det \boldsymbol{J}_0}{\det \boldsymbol{J}} (\boldsymbol{T}_S^0)^{-1} \begin{bmatrix} \xi^1 & \xi^1\xi^2 & 0 & 0 & 0 & 0 & 0 \\ 0 & 0 & \xi^2 & \xi^1\xi^2 & 0 & 0 & 0 \\ 0 & 0 & 0 & 0 & \xi^3 & \xi^1\xi^3 & \xi^2\xi^3 \\ 0 & 0 & 0 & 0 & 0 & 0 & 0 \\ 0 & 0 & 0 & 0 & 0 & 0 & 0 \\ 0 & 0 & 0 & 0 & 0 & 0 & 0 \end{bmatrix} \quad , \tag{18}$$

$$\boldsymbol{M}_{\vec{E}} = \frac{\det \boldsymbol{J}_0}{\det \boldsymbol{J}} \boldsymbol{J}_0^{-1} \begin{bmatrix} 0 & 0 & 0 \\ 0 & 0 & 0 \\ \xi^3 & \xi^1\xi^3 & \xi^2\xi^3 \end{bmatrix} \quad . \tag{19}$$

According to Eq. (19) the approximation of the electric field is a bi-linear function through the thickness.

The approximation of the independent field $\widetilde{\boldsymbol{\sigma}}$ is defined as

$$\widetilde{\boldsymbol{\sigma}}_e^h = \boldsymbol{M}_\beta \boldsymbol{\beta} \quad \text{with} \quad \boldsymbol{M}_\beta = \begin{bmatrix} \boldsymbol{N}_S & \mathbf{0} \\ \mathbf{0} & \boldsymbol{N}_{\vec{D}} \end{bmatrix} \quad \text{and} \quad \boldsymbol{\beta} \in \mathbb{R}^{30} \quad . \tag{20}$$

Here the matrix $\boldsymbol{N}_S$ is equivalent to $\boldsymbol{N}_E$ of Eq. (18), where instead $(\boldsymbol{T}_E^0)^T$ the transformation matrix $(\boldsymbol{T}_S^0)^T$ is used. The interpolation $\boldsymbol{N}_{\vec{D}}$ is identical to $\boldsymbol{N}_{\vec{E}}$.

Considering the above interpolations in Eqs. (6) and (8) one obtains the following matrices

$$\begin{aligned} \boldsymbol{A}_e^{ij} &= \int_{\mathcal{B}_e} (\boldsymbol{M}_\alpha^i)^T \, \mathbb{D} \, \boldsymbol{M}_\alpha^j \, \mathrm{dV_e} & \boldsymbol{C}_e &= \int_{\mathcal{B}_e} (\boldsymbol{M}_\alpha^1)^T \, \boldsymbol{M}_\beta \\ \boldsymbol{L}_e &= \int_{\mathcal{B}_e} \boldsymbol{B}^T \, \boldsymbol{M}_\beta \, \mathrm{dV_e} & \boldsymbol{K}_e &= \int_{\mathcal{B}_e} \boldsymbol{G} \, \mathrm{dV_e} \end{aligned} \tag{21}$$

and vectors

$$\begin{aligned} \boldsymbol{a}_e^i &= \int_{\mathcal{B}_e} (\boldsymbol{M}_\alpha^i)^T \, (\boldsymbol{\sigma} - \widetilde{\boldsymbol{\sigma}}) \, \mathrm{dV_e} & \boldsymbol{b}_e &= \int_{\mathcal{B}_e} \boldsymbol{M}_\beta^T \, (\boldsymbol{\varepsilon} - \bar{\boldsymbol{\varepsilon}}) \, \mathrm{dV_e} \\ \boldsymbol{f}_e^{int} &= \int_{\mathcal{B}_e} \boldsymbol{B}^T \, \widetilde{\boldsymbol{\sigma}} \, \mathrm{dV_e} & \boldsymbol{f}_e^{ext} &= \int_{\mathcal{B}_e} \boldsymbol{N}^T \, \widetilde{\boldsymbol{p}} \, \mathrm{dV_e} + \int_{\partial\mathcal{B}_e} \boldsymbol{N}^{\mathrm{T}} \, \widetilde{\boldsymbol{t}} \, \mathrm{dA_e} \, , \end{aligned} \tag{22}$$

with $i = 1,2$ and $j = 1,2$. In Eq. (22) the body and surface loads are determined by $\widetilde{\boldsymbol{p}}^T = [\boldsymbol{b}^T,\, 0]$ and $\widetilde{\boldsymbol{t}}^T = [\boldsymbol{t}^T,\, q]$. Having in mind that Eq. (6) is solved iteratively the following approximation on element level is obtained

$$
\begin{aligned}
&\left[\delta\Pi + \mathrm{D}[\delta\Pi]\cdot(\Delta\boldsymbol{u},\,\Delta\phi,\,\Delta\bar{\boldsymbol{\varepsilon}},\,\Delta\widetilde{\boldsymbol{\sigma}})\right]_e^h \Rightarrow \\
&\begin{bmatrix} \delta\boldsymbol{v}_e \\ \delta\boldsymbol{\alpha}_e^1 \\ \delta\boldsymbol{\alpha}_e^2 \\ \delta\boldsymbol{\beta}_e \end{bmatrix}^T \left(\begin{bmatrix} \boldsymbol{f}_e^{int} - \boldsymbol{f}_e^{ext} \\ \boldsymbol{a}_e^1 \\ \boldsymbol{a}_e^2 \\ \boldsymbol{b}_e \end{bmatrix} + \begin{bmatrix} \boldsymbol{K}_e & \boldsymbol{0} & \boldsymbol{0} & \boldsymbol{L}_e \\ \boldsymbol{0} & \boldsymbol{A}_e^{11} & \boldsymbol{A}_e^{11} & -\boldsymbol{C}_e \\ \boldsymbol{0} & \boldsymbol{A}_e^{21} & \boldsymbol{A}_e^{22} & \boldsymbol{0} \\ \boldsymbol{L}_e^T & -\boldsymbol{C}_e^T & \boldsymbol{0} & \boldsymbol{0} \end{bmatrix} \begin{bmatrix} \Delta\boldsymbol{v}_e \\ \Delta\boldsymbol{\alpha}_e^1 \\ \Delta\boldsymbol{\alpha}_e^2 \\ \Delta\boldsymbol{\beta}_e \end{bmatrix} \right) .
\end{aligned}
\tag{23}
$$

Taking into account that the finite element interpolations for the fields $\bar{\boldsymbol{\varepsilon}}$, $\widetilde{\boldsymbol{\sigma}}$ are discontinuous across the element boundaries a condensation on element level yields the element stiffness matrix and the right hand side vector

$$
\begin{aligned}
\boldsymbol{K}_{Te} &= \boldsymbol{K}_e + \boldsymbol{L}_e \boldsymbol{C}_e^{-1}\, \boldsymbol{A}_e\, \boldsymbol{C}_e^{-T} \boldsymbol{L}_e^T \\
\boldsymbol{f}_e &= \boldsymbol{f}_e^{ext} - \boldsymbol{f}_e^{int} - \boldsymbol{L}_e \boldsymbol{C}_e^{-1}\, \boldsymbol{A}_e\, \boldsymbol{C}_e^{-T}\, \boldsymbol{b}_e - \boldsymbol{L}_e \boldsymbol{C}_e^{-1}\, \boldsymbol{a}_e \quad ,
\end{aligned}
\tag{24}
$$

with $\boldsymbol{A}_e = \boldsymbol{A}_e^{11} - \boldsymbol{A}_e^{12}(\boldsymbol{A}_e^{22})^{-1}\boldsymbol{A}_e^{21}$ and $\boldsymbol{a}_e = \boldsymbol{a}_e^1 - \boldsymbol{A}_e^{12}(\boldsymbol{A}_e^{22})^{-1}\boldsymbol{a}_e^2$. After assembly over all elements $\boldsymbol{K}_T = \mathsf{A}_{e=1}^{nelm}\, \boldsymbol{K}_{Te}$, $\Delta\boldsymbol{V} = \mathsf{A}_{e=1}^{nelm}\, \Delta\boldsymbol{v}_e$ and $\boldsymbol{F} = \mathsf{A}_{e=1}^{nelm}\, \boldsymbol{f}_e$ one obtains

$$
\boldsymbol{K}_T\, \Delta\boldsymbol{V} = \boldsymbol{F}
\tag{25}
$$

with the unknown incremental nodal displacements and the electric potential. The update of the internal degrees of freedoms reads

$$
\begin{aligned}
\Delta\boldsymbol{\alpha}_e^1 &= \boldsymbol{C}_e^{-T} \boldsymbol{L}_e^T \Delta\boldsymbol{v} + \boldsymbol{C}_e^{-T} \boldsymbol{b}_e \\
\Delta\boldsymbol{\alpha}_e^2 &= -(\boldsymbol{A}_e^{22})^{-1} \boldsymbol{a}_e^2 - (\boldsymbol{A}_e^{22})^{-1} \boldsymbol{A}_e^{21} \Delta\boldsymbol{\alpha}_e^1 \\
\Delta\boldsymbol{\beta}_e &= \boldsymbol{C}_e^{-1} \boldsymbol{A}_e \Delta\boldsymbol{\alpha}_e^1 + \boldsymbol{C}_e^{-1} \boldsymbol{a}_e \quad .
\end{aligned}
\tag{26}
$$

6 Numerical Examples

The developed solid shell element formulation is implemented in a modified version of the program FEAP [24]. Some numerical examples are chosen to demonstrate the accurate behavior of the proposed element. Furthermore the examples demonstrate the ability of the present solid shell element to analyze piezoelectric devices.

6.1 Patch tests

The patch tests are well known in structural mechanics, see e.g. [25]. Here, we adopt the classical mechanical patch tests and extend them to the piezoelectric finite element formulation. The test is fulfilled if the finite element formulation is able to reproduce constant stresses along with constant strains and a constant electric field for disturbed element geometries. In addition the piezoelectric element should be able to represent constant dielectric displacements. The patch tests are an important and necessary condition for convergence with respect to mesh refinement.

Furthermore we discuss the impact of the interpolation (19) to the patch test. In detail two element formulations are considered, which differ in the interpolation Eq. (19). The present formulation is denoted by HSE and HSE-0 is a formulation without $\boldsymbol{M}_{\vec{E}}$.

For shell structures it is distinguished between the membrane patch test and the out of plane bending patch test. In both tests we consider the element mesh illustrated in Fig. 1, which was introduced in [25]. The boundary conditions are chosen as follows: at $X_1 = 0$ all displacements are fixed and at $X_3 = -t/2$ the electric potential φ is set to zero. The system is subjected to different nodal forces F_u and F_l, which are described below. For the calculation of the two patch tests a geometrically linear behavior is assumed.

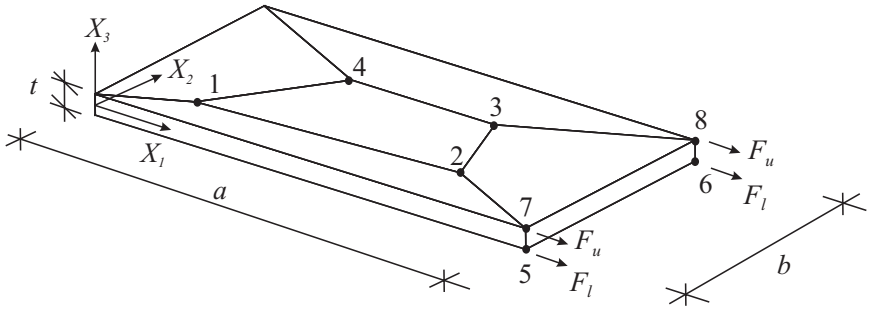

Geometry data:			Nodal coordinates: (X_1, X_2, X_3)			
a	=	0.24 m	1 :	(0.04,	0.02,	0.005)
b	=	0.12 m	2 :	(0.18,	0.03,	0.005)
t	=	0.01 m	3 :	(0.16,	0.08,	0.005)
			4 :	(0.08,	0.08,	0.005)

Figure 1: Element mesh for the patch tests and interior nodes 1, 2, 3, 4 on top of the surface

For the sake of simplicity and without loss of generality we assume a simplified piezoelectric material; the isotropic elastic material and the piezoelectric moduli are summarized in Tab. 1. It is noted that the material parameters correspond to the global cartesian coordinate system $\boldsymbol{e}_i$. Accordingly the local basis system $\boldsymbol{t}_i$ in Section 2 is substituted by $\boldsymbol{e}_i$.

$E_1 = E_2 = E_3 = 123 \cdot 10^9\,\mathrm{N/m^2}$, $G_{12} = G_{13} = G_{23} = 61.5 \cdot 10^9\,\mathrm{N/m^2}$
$\mathfrak{e}_{13} = -5\,\mathrm{C/m^2}$, $\epsilon_{11} = \epsilon_{22} = \epsilon_{33} = 12.5 \cdot 10^{-9}\,\mathrm{C/Nm^2}$

Table 1: Simplified material properties; not listed parameters are zero

6.1.1 Membrane patch tests

In this example we apply $F_u = F_l = 3 \cdot 10^4$ N, which produces a constant stress in X_1-direction as $S_{11} = 1 \cdot 10^8\,\mathrm{N/m^2}$. With respect to the above introduced material properties the problem is degenerated to a 1D problem, which is determined by two constitutive equations in X_1 direction. With respect to the boundary conditions an analytical solution leads to

$u_1 = 1.92 \cdot 10^{-4}$ m, $u_2 = u_3 = 0$ at $X_1 = 0.24$ m and $\varphi = 3.2 \cdot 10^3$ V at the surface $X_3 = 0.005$ m. The results of a numerical solution of the problem with the above introduced elements are shown in Tab. 2. The stress and the dielectric displacement are calculated in a postprocess and are obtained as constant in the hole domain. For both element formulations they read $\widetilde{S}_{11} = 1 \cdot 10^8$ N/m^2 and $\widetilde{\vec{D}}_1 = 0$ C/m^2. All results are in accordance with the analytical solution, which confirms that the membrane patch test is passed. It is noted that the enhanced assumed gradient interpolation Eq. (19) is not necessary to pass this test.

		all nodes at	HSE-0	HSE	analytical
u_1	[m]	$X_1 = 0.24$m	$1.92 \cdot 10^{-4}$	$1.92 \cdot 10^{-4}$	$1.92 \cdot 10^{-4}$
φ	[V]	$X_3 = 0.005$m	$3.20 \cdot 10^3$	$3.20 \cdot 10^3$	$3.20 \cdot 10^3$

Table 2: Solutions for displacements and electric potential in membrane patch test

6.1.2 Out-of-plane bending patch test

The purpose of this test is to receive a constant bending stress. Therefore the system is subjected to the loads $F_u = -1 \cdot 10^5$ N and $F_l = +1 \cdot 10^5$ N, which results in a stress constant in X_1 direction and linear in X_3 $S_{11} = -2 \cdot 10^{11} X_3$ N/m^2. An analytical calculation yields a tip deflection $u_3 = 0.8 X_1^2$ and an electric potential $\varphi = 0.32 X_3^2 - 8 \cdot 10^{-6}$; evaluated at $X_1 = 0.24$ m and $X_3 = 0.005$ m yields $u_3 = 4.608 \cdot 10^{-2}$ m, $\varphi = 0$ V. It is noted that the analytical distribution of the electric potential is a quadratic function through the thickness. The reason therefore is that the applied couple force produces a linear stress distribution S_{11} through the thickness. With respect to the constitutive equations and the material properties Tab. 1 it follows a linear strain distribution E_{11} and a linear electric field distribution $\vec{E}_3$ through the thickness. The electric potential is obtained by integrating the electric field considering the boundary conditions. It turns out that the electric potential is a quadratic function through the thickness, which is zero at the top and bottom surface. In Tab. 3 the displacement u_3 at the free edge of the plate and the electric potential at the top surface are shown.

	all nodes at	HSE-0	HSE	analytical
u_3 [m]	$X_1 = 0.24$m	$4.68293 \cdot 10^{-2}$	$4.60800 \cdot 10^{-2}$	$4.60800 \cdot 10^{-2}$
φ [V]	$X_3 = 0.005$m	≈ 0	≈ 0	0

Table 3: Solutions for displacements and electric potential in bending patch test

It is found that the HSE solid shell element provides correct results. The HSE-0 without any assumed gradient interpolations leads to a constant deflection, but this is larger than the analytical solution. This effect may be explained by considering the remaining interpolation matrix $\boldsymbol{N}_{\vec{E}}$ Eq. (17). It determines $\vec{E}_3$ as a bilinear function of ξ^1 and ξ^2 and constant in thickness direction ξ^3. Hence, it is not possible to approximate a linear distribution of $\vec{E}_3$ through the thickness. As a result the electric field is approximated as zero. Consequently the strain $\bar{E}_{11}$ is overestimated to obtain the linear stress distribution S_{11}, which leads to the pure mechanical solution without any piezoelectric coupling.

6.2 Piezoelectric buckling

In this example the buckling behavior of a piezoelectric plate is analyzed. The numerical results are compared with those proposed in [16]. A square plate consisting out of six layers is considered; the layup and the geometrical data of the plate are given in Fig. 2. The principal directions of the graphite epoxy plies lie in the X_1-X_2 plane, where the angle is defined with respect to the X_1 axes, see Fig. 2. The plate is modeled by 16×16 elements in-plane and 6 elements through the thickness.

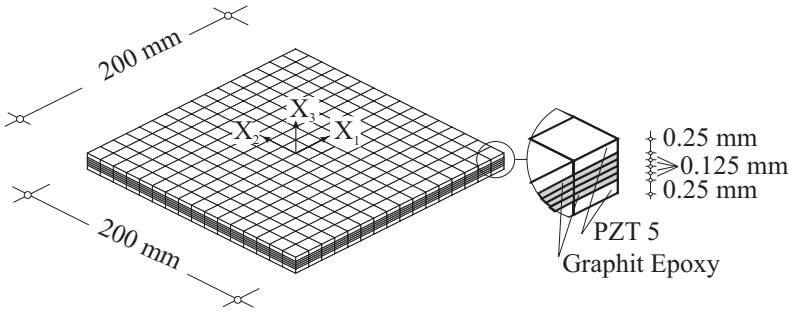

Figure 2: Finite element model of the laminated square plate with the stacking sequence of Graphite Epoxy $[0^o, 90^o, 90^o, 0^o]$

For the electrical loading an electric potential is applied to the upper and lower surface of the piezoelectric layers; where all three displacements of the middle surface at the boundary of the plate are fixed, see Fig. 3.

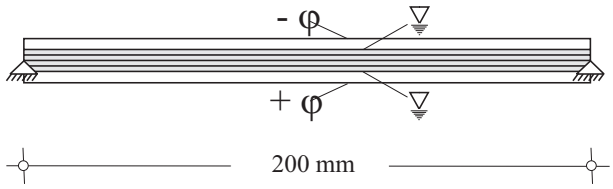

Figure 3: Applied electric potential and boundary conditions

According to [16] the material data are summarized in Tab. 4. The orientation of the fibers is chosen with respect to the X_1-direction. Due to the fact that the material constants in thickness direction are not required in the plate formulation of [16], they are assumed in the present work.

Piezoelectric buckling is observed by increasing the electric potential up to a critical value. With respect to the coupling matrix, see Tab. 4, an increasing negative electric field leads to negative values for the stresses in X_1 and X_2 directions, which cause a loss of stiffness. The first four buckling modes are calculated with the present solid shell element. The corresponding critical values of φ are listed in Tab. 5. The good agreement of the critical electric potentials confirms that the present solid shell element performs well within a piezoelectric buckling analysis.

The work of [16] is restricted to calculate the critical loads and buckling modes. With the present formulation the post buckling behavior is analyzed. This is important if the

Graphite Epoxy 0^o
$E_1 = E_2 = 132.4 \cdot 10^9\,\mathrm{N/m^2}$, $E_3 = 10.8 \cdot 10^9\,\mathrm{N/m^2}$
$\nu_{12} = \nu_{13} = 0.24$, $\nu_{23} = 0.49$
$G_{12} = G_{13} = 5.6 \cdot 10^9\,\mathrm{N/m^2}$, $G_{23} = 3.6 \cdot 10^9\,\mathrm{N/m^2}$
PZT-5 ceramic
$E_1 = 62.0 \cdot 10^9\,\mathrm{N/m^2}$, $E_2 = E_3 = 54.9 \cdot 10^9\,\mathrm{N/m^2}$
$\nu_{12} = \nu_{13} = \nu_{23} = 0.31$
$G_{12} = G_{13} = 23.6 \cdot 10^9\,\mathrm{N/m^2}$, $G_{23} = 18.0 \cdot 10^9\,\mathrm{N/m^2}$
$\mathbb{e}_{13} = \mathbb{e}_{23} = -12.006\,\mathrm{C/m^2}$, $\mathbb{e}_{33} = 17.277\,\mathrm{C/m^2}$, $\mathbb{e}_{51} = \mathbb{e}_{62} = 15.812\,\mathrm{C/m^2}$
$\epsilon_{11} = \epsilon_{22} = \epsilon_{33} = 22.99 \cdot 10^{-9}\,\mathrm{C^2/N\ m^2}$

Table 4: Material properties of the plate

order	1	2	3	4
present solid shell element	70.6	172.5	193.3	286.1
Varelis, Saravanos [16]	68.8	170.5	189.4	289.3

Table 5: Critical electric potential φ [V] for the first four buckling modes

piezoelectric plate is employed as a switch device. Here we introduce such a device by modifying the geometry of the considered plate slightly by changing the thickness of the upper Graphit Epoxy layer from 0.250 mm to 0.249 mm. This geometrical imperfection initializes the buckling direction, thus the stability problem becomes a pure bending problem.

In Fig. 4 the electric potential ϕ is plotted versus the vertical deflection at the center point of the plate. An increasing load from $\varphi = 60$ V to $\varphi = 120$ V leads to a large change in the center deflection $u_3 = 0.002$ mm to $u_3 = 0.731$ mm. This effect may be utilized for a switching device.

6.3 Telescopic actuator

Telescopic actuators consist of concentric shells interconnected by end caps which alternate in placement between the two axial ends of the shells, see Figure 5. The diameters in Figure 5 refer to the outside of the cylindric shells. The telescopic actuators are designed to accomplish for a high displacement actuation at the cost of force, see e. g. [26]. The fabrication and the static behavior is analyzed in [27, 28].

The cascading shells are polarized in radial direction. The telescopic actuator consists of a piezoelectric ceramics; the material data are summarized in Table 6, where the piezoelectric constants $\mathbb{d}_{13}$ and $\mathbb{d}_{33}$ are taken form [27] and all other quantities are assumed. The orientation of the local basis system $\boldsymbol{t}_i$ is defined by $\boldsymbol{t}_1$ in circumferential direction, $\boldsymbol{t}_2$ in axial direction and $\boldsymbol{t}_3$ in radial direction.

With respect to symmetry only a quarter of the system is modeled by finite elements. For each cylinder 5 elements in axial direction, 1 element through the thickness and 12 elements in circumferential directions are applied. The end caps are modeled by 3 elements through the thickness. The finite element model is shown in Fig. 5. The system is supported in X_3-

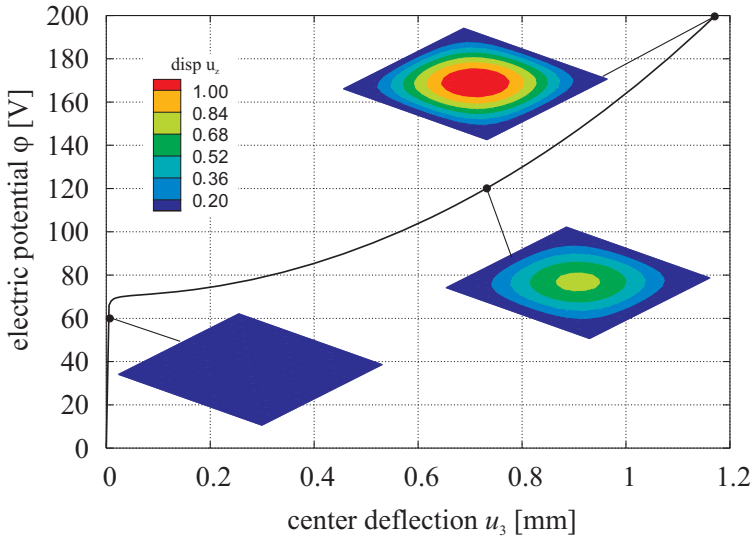

Figure 4: Load deflection curve and plots of the vertical deflection at characteristic points

$E_1 = E_2 = 60.61 \cdot 10^9\,\mathrm{N/m^2}$, $E_3 = 48.31 \cdot 10^9\,\mathrm{N/m^2}$
$\nu_{23} = \nu_{13} = 0.41$, $\nu_{12} = 0.29$
$G_{23} = G_{13} = 22.99 \cdot 10^9\,\mathrm{N/m^2}$, $G_{12} = 23.47 \cdot 10^9\,\mathrm{N/m^2}$
$\mathrm{e}_{13} = \mathrm{e}_{23} = -29.878\,\mathrm{C/m^2}$, $\mathrm{e}_{33} = 10.631\,\mathrm{C/m^2}$, $\mathrm{e}_{51} = \mathrm{e}_{62} = 17.034\,\mathrm{C/m^2}$
$\epsilon_{11} = \epsilon_{11} = 15.09 \cdot 10^{-9}\,\mathrm{C^2/N\ m^2}$ $\epsilon_{11} = 14.16 \cdot 10^{-9}\,\mathrm{C^2/N\ m^2}$

Table 6: Telescopic actuator: material properties

direction at the lower bottom at the outside edge and it is is loaded by applying an electric potential to the piezoelectric cylindrical shells in such a way that some cylinders are expanded and some are shortened in axial direction. The applied electric potential and the deformed configuration is depicted in Figure 6.

The load deflection behavior of the axial displacements for the different cylinders, see Figure 5, are depicted in Figure 7. A comparison to the experimental data in [27] shows good agreement, which is very promising for analyzing arbitrary piezoelectric shells with the present element formulation.

7 Conclusion

In this paper a geometrically nonlinear solid shell element to analyze piezoelectric structures is presented. The finite element formulation is based on a mixed variational principle including six independent field variables. An efficient finite element implementation is presented. The geometrically nonlinear theory allows large deformations and includes the analysis of stability problems. The multi-field formulation passes the relevant patch tests, which are well known from structural mechanics. Some numerical examples show the applicability of the proposed element to geometrically nonlinear and linear problems.

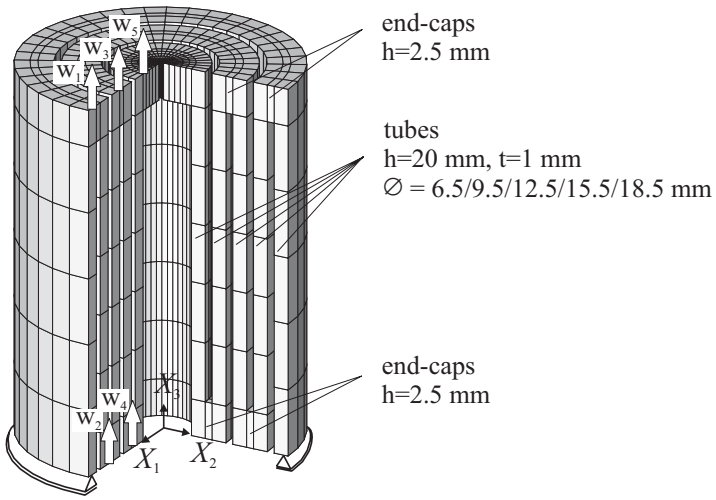

Figure 5: Telescopic actuator: system, boundary conditions and finite element model

A Material properties

In this Appendix the material properties which arise due to a polarization in the local $\boldsymbol{t}_3$ direction are summarized. Relating to $\boldsymbol{t}_i$ the inverse elasticity matrix and the piezoelectric matrix $\mathbb{e}$ are given as

$$\mathbb{C}^{-1} = \begin{bmatrix} \frac{1}{E_1} & -\frac{\nu_{12}}{E_2} & -\frac{\nu_{13}}{E_3} & 0 & 0 & 0 \\ -\frac{\nu_{12}}{E_2} & \frac{1}{E_2} & -\frac{\nu_{23}}{E_3} & 0 & 0 & 0 \\ -\frac{\nu_{13}}{E_3} & -\frac{\nu_{23}}{E_3} & \frac{1}{E_3} & 0 & 0 & 0 \\ 0 & 0 & 0 & \frac{1}{G_{12}} & 0 & 0 \\ 0 & 0 & 0 & 0 & \frac{1}{G_{13}} & 0 \\ 0 & 0 & 0 & 0 & 0 & \frac{1}{G_{23}} \end{bmatrix}, \quad \mathbb{e} = \begin{bmatrix} 0 & 0 & \mathbb{e}_{13} \\ 0 & 0 & \mathbb{e}_{23} \\ 0 & 0 & \mathbb{e}_{33} \\ 0 & 0 & 0 \\ \mathbb{e}_{51} & 0 & 0 \\ 0 & \mathbb{e}_{62} & 0 \end{bmatrix}. \tag{27}$$

The elastic moduli E_1, E_2, E_3, the Poisson's ratios ν_{12}, ν_{13}, ν_{23} and the shear moduli G_{12}, G_{13}, G_{23} are material parameters. They are defined together with the piezoelectric constants in Section 6. The permittivity matrix has diagonal form and is characterized by ϵ_{11}, ϵ_{22} and ϵ_{33}.

References

[1] D. Varelis, D. Saravanos, Coupled mechanics and finite element for non-linear laminated piezoelectric shallow shells undergoing large displacements and rotations, Smart Materials and Structures 11 (2002) 330–336. 1

[2] M. Kögel, M. Bucalem, Locking-free piezoelectric MITC shell elements, in: K. Bathe (Ed.), Computational Fluid and Solid Mechanics, Elsevier Science, Oxford, 2003, pp. 392–395. 1

[3] M. Bernadou, C. Haenel, Modelization and numerical approximation of piezoelectric thin shells. part I: The continuous problems, Computer Methods in Applied Mechanics and Engineering 192 (2003) 4003–4043. 1

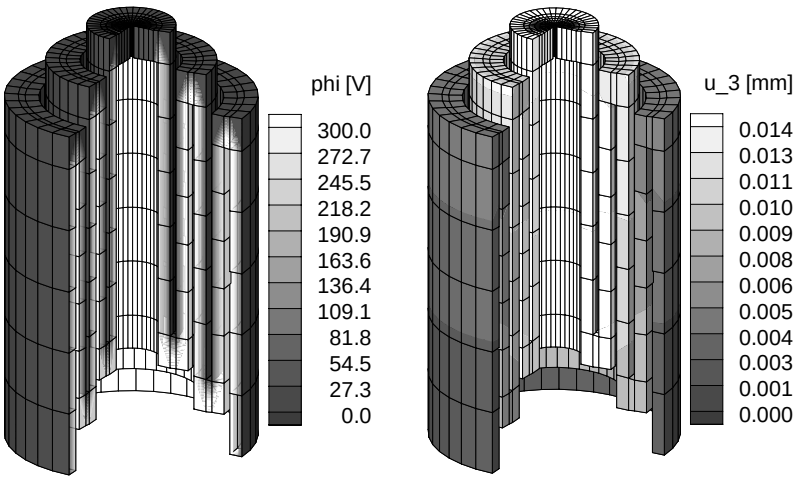

Figure 6: Telescopic actuator: deformed configuration with a plot of the electric potential and the axial displacement

[4] M. Bernadou, C. Haenel, Modelization and numerical approximation of piezoelectric thin shells. part II: Approximation by finite element methods and numerical experiments, Computer Methods in Applied Mechanics and Engineering 192 (2003) 4045–4073. 1

[5] R. Lammering, S. Mesecke-Rischmann, Multi-field variational formulations and related finite elements for piezoelectric shells, Smart Materials and Structures 12 (2003) 904–913. 1

[6] X. Wang, Y. Wang, On non-linear behaviour o spherical shallow shells bonded with piezoelectric actuators by the differential quadrature element method (DQEM), International Journal for Numerical Methods in Engineering 53 (2002) 1477–1490. 1

[7] S. Klinkel, W. Wagner, A geometrically non-linear piezoelectric solid shell element based on a mixed multi-field variational formulation, International Journal for Numerical Methods in Engineering 65 (3) (2006) 349–382. 1

[8] X. Tan, L. Vu-Quoc, Optimal solid shell element for large deformable composite structures with piezoelectric layers and active vibration control, International Journal for Numerical Methods in Engineering 64 (2005) 1981–2013. 1

[9] S. Zheng, X. Wang, W. Chen, The formulation of a refined hybrid enhanced assumed strain solid shell element and its application to model smart structures containing distributed piezoelectric sensors/actuators, Smart Materials and Structures 13 (2004) N43–N50. 1

[10] K. Sze, L. Yao, A hybrid stress ANS solid-shell element and its generalization for smart structure modelling. part I – solid-shell element formulation, International Journal for Numerical Methods in Engineering 48 (2000) 545–564. 1

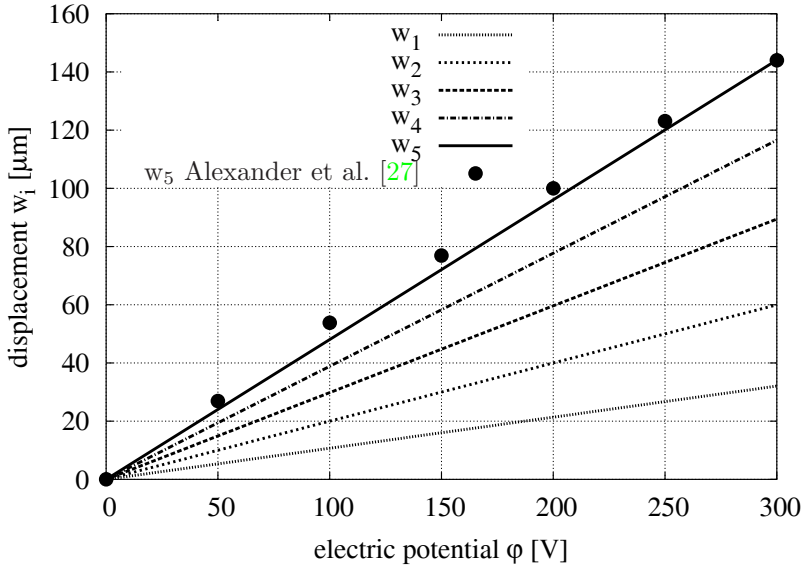

Figure 7: Electric potential versus axial deflections of the different cylinders

[11] K. Sze, L. Yao, S. Yi, A hybrid stress ANS solid-shell element and its generalization for smart structure modelling. part II – smart structure modelling, International Journal for Numerical Methods in Engineering 48 (2000) 565–582. 1

[12] K. Sze, L. Yao, Modelling smart structures with segmented piezoelectric sensors and actuators, Journal of Sound and Vibration 253 (2000) 495–520. 1

[13] Y. Zhou, H. Tzou, Active control of nonlinear piezoelectric circular shallow spherical shells, International Journal of Solids and Structures 37 (2000) 1663–1677. 1

[14] H. Tzou, Y. Bao, Nonlinear piezothermoelasticity and multi-field actuations, part 1: Nonlinear anisotropic piezothermoelastic shell elements, Journal of Vibration and Acoustics 119 (1997) 374–381. 1

[15] H. Tzou, Y. Zhou, Nonlinear piezothermoelasticity and multi-field actuations, part 2: Control of nonlinear deflection, buckling and dynamics, Journal of Vibration and Acoustics 119 (1997) 382–389. 1

[16] D. Varelis, D. Saravanos, Nonlinear coupled mechanics and initial buckling of composite plates with piezoelectric actuators and sensors, Smart Materials and Structures 11 (2002) 330–336. 1, 6.2, 6.2, 6.2, 6.2

[17] A. Benjeddou, J. Deü, S. Letombe, Free vibrations of simply-supported piezoelectric adaptive plates: An exact sandwich formulation, Thin-Walled Structures 40 (2002) 573–593. 1

[18] M. Bernadou, C. Haenel, Modelization and numerical approximation of piezoelectric thin shells. part III: From the patches to the active structures, Computer Methods in Applied Mechanics and Engineering 192 (2003) 4075–4107. 1

[19] S. Miranda, F. Ubertini, Consistency analysis of electroelastic finite element models, in: Proc., 2nd European Conference on Computational Mechanics, Cracow, 2001, pp. CD–Version. 1

[20] K. Sze, Y. Pan, Hybrid finite element models for piezoelectric materials, Journal of Sound and Vibration 226 (1999) 519–547. 1

[21] S. Klinkel, F. Gruttmann, W. Wagner, A robust non-linear solid shell element based on a mixed variational formulation, Computational Methods in Applied Mechanics and Engineering 195 (1-3) (2006) 179–201. 1

[22] E. Dvorkin, K. Bathe, A continuum based four–node shell element for general nonlinear analysis, Engineering Computations 1 (1984) 77–88. 5

[23] P. Betsch, E. Stein, An assumed strain approach avoiding artificial thickness straining for a nonlinear 4–node shell element, Communications in Numerical Methods in Engineering 11 (1995) 899–909. 5

[24] R. Taylor, Feap - manual, http:\\www.ce.berkeley\ ∼rlt\feap\manual.pdf. 6

[25] R. MacNeal, R. Harder, A proposed standard set of problems to test finite element accuracy, Finite Elemets in Analysis and Design 1 (1985) 3–20. 6.1

[26] C. Niezrecki, D. Brei, S. Balakrishnan, A. Moskalik, Piezoelectric actuation: State of the art, The Shock and Vibration Digest 33 (4) (2001) 269–280. 6.3

[27] P. Alexander, D. Brei, W. Miao, J. Halloran, Fabrication and experimental characterization of d_{31} telescopic piezoelectric actuators, Journal of Material Science 36 (2001) 4231–4237. 6.3, 6.3

[28] D. Brei, N. Berner, P. Alexander, Modeling and study of the quasi-static behavior of piezoceramic telescopic actuation architectures, Journal of Intelligent Material Systems and Structures 12 (2001) 303–313. 6.3